

# A Dataset and Method for Hallux Valgus Angle Estimation Based on Deep Learning

Ningyuan Xu<sup>a,b,1</sup>, Jiayan Zhuang<sup>b,\*1</sup>, Yaojun Wu<sup>c,d</sup> and Jiangjian Xiao<sup>b</sup>

<sup>a</sup>University of Chinese Academy of Sciences, No.19 Yuquan Road, Shijingshan District, Beijing, China

<sup>b</sup>Ningbo Institute of Industrial Technology, Chinese Academy of Sciences, No.1219, Zhongguan West Road, Zhenhai District, Ningbo City, Zhejiang Province, China

<sup>c</sup>Hwa Mei Hospital, University of Chinese Academy of Sciences, 41 Northwest Street, Ningbo City, Zhejiang Province, China

<sup>d</sup>Ningbo Institute of Life and health Industry, University of Chinese Academy of sciences

## ARTICLE INFO

**Keywords:**

hallux valgus  
deep learning  
image processing  
x-ray

## ABSTRACT

Angular measurements is essential to make a reasonable treatment for Hallux valgus (HV), a common forefoot deformity. However, it still depends on manual labeling and measurement, which is time-consuming and sometimes unreliable. Automating this process is a thing of concern. However, it lack of dataset and the keypoints based method which made a great success in pose estimation is not suitable for this field. To solve the problems, we made a dataset and developed an algorithm based on deep learning and linear regression. It shows great fitting ability to the ground truth.

## 1. Introduction

Hallux valgus (HV) is a common forefoot deformity characterized by a valgus deviation of the great toe and varus deviation of the first metatarsal[1]. Its prevalence increases with age, and it afflicts 3.5% of adolescents, 23% of adults aged 18-65 years and 35.7% of adults aged 65 years and older[2, 3]. Patients with HV typically complain of over forefoot pain, intolerance of shoe wear, impaired gait patterns or falls among the aged[4, 5, 6, 7]. Up to date, there have been more than 100 different operative techniques defined for hallux valgus[8]. The proper selection of various operative procedures is commonly based on X-ray angular measurement of the foot before operation, including the hallux valgus angle (HVA), the inter metatarsal angle (IMA), and the distal metatarsal articular angle (DMAA)[9]. According to the range of HVA and IMA, the severity of HV can be classified into three types[10]:

1. mild( $15^\circ \leq \text{HVA} \leq 20^\circ$ ,  $9^\circ \leq \text{IMA} \leq 11^\circ$ )
2. moderate ( $21^\circ \leq \text{HVA} \leq 39^\circ$ ,  $12^\circ \leq \text{IMA} \leq 17^\circ$ )
3. severe ( $\text{HVA} \geq 40^\circ$ ,  $\text{IMA} \geq 18^\circ$ )

In order to make applicable treatment decisions, angular measurements must be accurate, reliable, and reproducible. However, traditional X-ray measurements may be inaccurate because they are influenced by variations in measurement techniques, and technicians' level of experience and ability to read X-ray images[11]. Numerous studies have showed intra observer and inter observer measurement errors[11, 12, 13, 14, 15]. At present, the common practice of orthopedic surgeons is just like Fig 1 (a) shows:

1. Draw the four auxiliary points of each phalanx.

\*Corresponding author

✉ xuningyuan@nimte.ac.cn (N. Xu); zhuangjiayan@nimte.ac.cn (J. Zhuang); wyj3247@163.com (Y. Wu); xiaojiangjian@nimte.ac.cn (J. Xiao)  
ORCID(s): 0000-0002-5977-0187 (N. Xu); 0000-0002-8350-6116 (J. Zhuang)

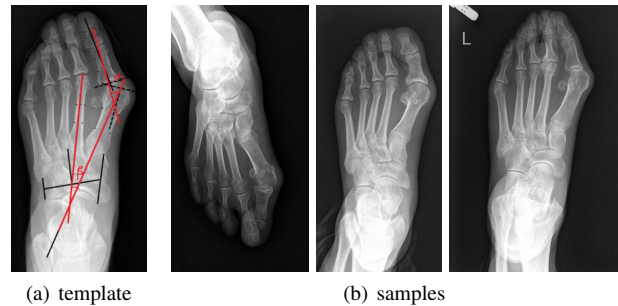


**Figure 1:** Samples of Hallux valgus, (a) is a template labeled by doctor; (b) is several samples of our dataset

2. Draw the center lines of each phalanx.
3. Measure the angles of the center lines.

The whole process stays in the manual stage, which is very complicated. At present, deep learning has made breakthroughs in many related fields, such as human posture recognition and gesture recognition. But there is no articles about hallux valgus angle estimation(HVAE) with deep learning. HVAD has difficulties as follows:

- To date, there is no publicly available dataset for HVA estimation.
- The domain of x-ray is different with natural image. X-ray is grayscale image, while natural image is based on RGB. So the models pretrained on large open datasets like ImageNet and COCO can't be well migrated to an X-Ray scene.
- The Method based on the key points is not suitable with the scenario. Once the key points are off by a few pixels, the angle of the whole line will be greatly offset. A deviation of a few pixels is acceptable for key-point detection but not for angle estimation.

**Table 1**  
Advantages and Disadvantages of Regression Based Method and Heatmap Based Method

Framework	Advantage	Disadvantage
Direct regression based	Quick and direct, trained with an end-end fashion. Easy to be extended to 3D scenarios.	Difficult to learn mapping. Hard to be applied to multi-person case.
Heatmap-based	Easy to be visualized. Robust to complicated case.	Large memory consumption for getting high resolution heat map. Hard to be extended to 3D scenarios.

our contribution is as follows:

- We are the first to use artificial intelligence to replace the traditional manual measurement of HVA and IMA.
- we made a HV dataset which collect from 143 patients and contains 235 preoperative images.
- We proposed a novel method based on neural network and traditional geometry. Compared to those method based on key points, our method can get more accurate estimation of HVA and IMA.

## 2. Related Works

Similar to the problem studied in this paper are human pose estimation, animal pose estimation, face landmark detection, hand pose estimation and so on. Traditional algorithms to deal with those problems used manual feature extraction and complex human model to obtain local representation and global pose structure.[16, 17] After deep learning brought great innovation to this field, the method can be grouped into two classes: One is based on regression,the other is based on heatmap. We will introduce the development of both method detaily in section 2.1 and section 2.2.

### 2.1. Models based on regression

The method based on regression attempts to learn the mapping from the image to the joint coordinates through the end-to-end framework and generally generates the joint coordinates directly.[18] However, predicting joint coordinates directly is very difficult with few constraints. So a more powerful network was introduced and the model structure was improved.Carreira *et al.* [19] proposed an iterative error feedback network based on GoogLeNet, which recursively processes the combination of input images and output results. The final results is improved from the initial coarse prediction. Sun *et al.* [20] proposed a structural perceptual regression method based on ResNet-50. The bone-based representation achieves more stable results by introduce body structure information than using joint position alone.

### 2.2. Models based on heatmap

Detection-based algorithms are dedicated to predicting the approximate position of body parts or joints[21], ground

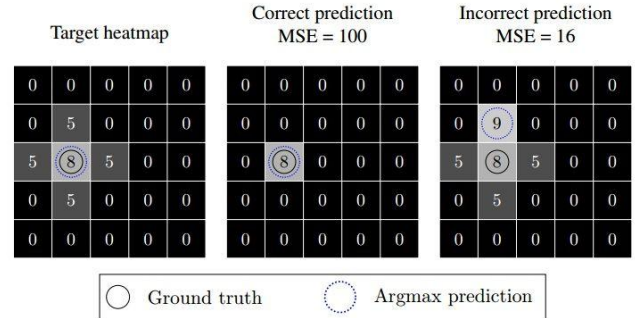


**Figure 2:** Inherent problems of Gaussian heatmap. The correct prediction have much bigger loss than incorrect prediction

truth is usually a series of heatmaps(a two-dimensional Gaussian distribution centered on joint coordinates to represent a joint position).[22] Although, obtaining joint coordinates from the heatmap is usually a non-differentiable process, which hinders the end-to-end training of the network[23], the heatmap representation is more robust than the coordinate representation, most recent studies are based on the heatmap representation.

To get more accurate results, Papandreou *et al.* [24] proposed an improved joint position representation, which is a combination of a binary activation heatmap and the corresponding position offset. In order to make better use of the input information, the structure of the neural network is very important. Some methods are mainly based on classical networks with appropriate improvements, such as multi-scale input network based on Googlenet [25] and deconvolution layer network based on ResNet [26].

In terms of iterative refinement, Somework has designed a multi-stage network to refine rough prediction results through end-to-end learning [27, 28, 21, 22, 29, 30]. Newell *et al.* [21] proposed a layered Hourglass architecture with residual modules as component units. Wei *et al.* [22] proposed a multi-stage prediction framework with input images for each stage. Yang*et al.* [29] designed a Pyramidal Residual Module (PRMS) to replace the Residual Module of Hourglass Network, and enhanced the cross-scale invariance of DCNN by learning features on different scales. Belagiannis and Zisserman[30] combine a 7-layer feedforward module with a recursive module to refine the results in an iterative manner. The model learns to predict joint and limb posi-

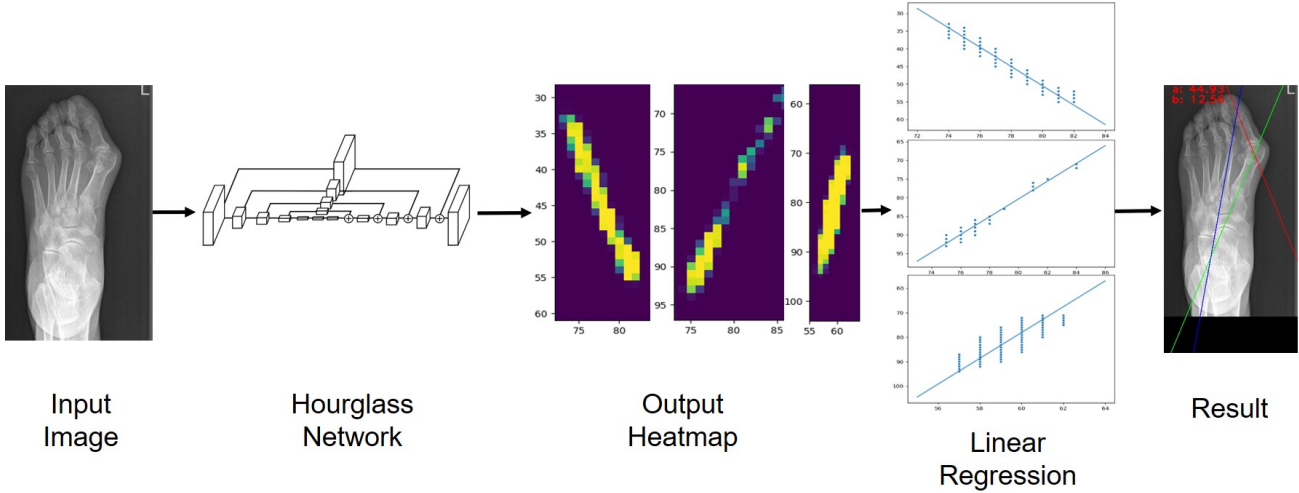


**Figure 3:** PipeLine of our method, our method is composed by neural network and linear regression. The neural network predicts three heatmaps from an input image, then the positions of points whose confidence is greater than 0.5 is picked up. The linear equations is calculated by linear regression on the points. With the linear equations, we can calculate the angles between the lines and visualize the result.

tion heatmaps. The relationship between the visibility of key points and the real imbalance of ground distribution is analyzed. In order to maintain a high resolution representation of features across the entire network, Sun *et al.* [31] proposed a new high resolution network with multi-scale feature fusion (HRNet).

As shown in 1, both of two methods have their own advantages and disadvantages. Direct regression learning for a single point is a highly nonlinear problem and lacks robustness, while heatmap learning is supervised by dense pixel information, so its robustness is better. However, compared with the original image size, the resolution of the heatmap representation is much lower due to the pooling operation in CNN, which limits the accuracy of the joint coordinate estimation. What is worse, as Fig 2 shows, Gaussian heatmap can sometimes bias the optimization direction of the network, and get wrong results. Luckily, our method can effectively avoid the influence of a few deviations on the final prediction results.

### 3. Method

The Pipeline of our method is as Fig 3 shows. It's based on deep learning and traditional geometry. In total, it can be divided into two parts: neural network and linear regression.

#### 3.1. Neural Network

Our method adopts the classic Hourglass neural network [21] in the field of key point detection. Compared with other known backbones, such as Vgg16, Vgg19, ResNe, DenseNet, the advantages of HG network lies in its symmetrical decoding and encoding structure, which will output the heatmap zoom back to a quarter of the original size, it can effectively improve the accuracy of predicting the keypoints. When a line only depends on two keypoints, the pixel-level deviation of keypoints can lead to a large deviation of the inclination of the whole line, which make the deviation of the results

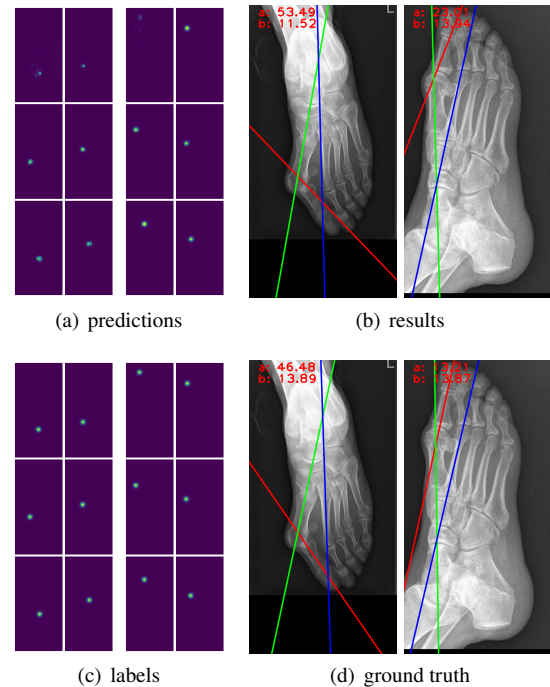


**Figure 4:** The results of keypoints-based method. Fig (a) is the predicted heatmaps of keypoint detection model; (b) is the final results; (c) is the labels for keypoints detection model; (d) is the ground truth.

intolerable. Even in the training dataset, the results are not ideal. As Fig 4 shows, the predicted heatmaps is closed with the labels in general position, but there is still pixel-level deviation, which lead the red lines on Fig 4 (b) deviated a lot compared to ground truth. The deviation of  $\alpha$  reach around  $7^\circ$  and  $10^\circ$ . To improve the situation, the first thing come to our mind is to take more keypoints. As Fig 5 shows, we

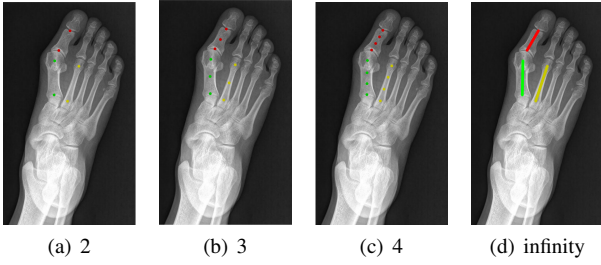


**Figure 5:** Different Numbers of Keypoints of a Line Segment

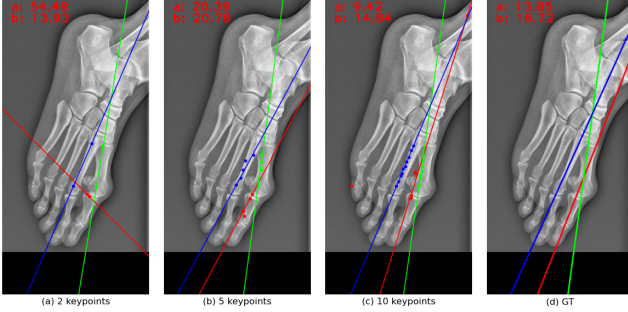


**Figure 6:** Comparison of Results Based on Different Numbers of Keypoints

can change numbers of the keypoints to 3, 4 and more. The results are also getting better as Fig 6 shows. But what if we take a limit on this case: filling in all the points between the two endpoints. It will certainly change into a line segment as Fig 5 (d) shows, and we don't need generate Gaussian heatmaps for every points since the number is enough to mitigate the nonlinearity. We can simply place all the points of a line segment on one heatmap as Fig 7 (a) and (c) shows. The problem of single Keypoint prediction is changed into the problem of front background segmentation. Sigmoid activation function is used in the output layer to generate probabilities, the units whose probabilities greater than 0.5 are the foreground (corresponding to the line segment), while the others is the background. This method also makes the prediction result robust since the pre-background imbalance is alleviated.

More importantly, even if there are several points did not predict prospective, others correctly predicted can help fit the ideal linear equation by linear regression. As 7 shows, although only a little points of red ones are detected by neural network, the final results after linear regression is still very good and the deviations of angles is much smaller.

### 3.2. Linear Regression

In the part of linear regression, we first make a set of coordinates of units whose probabilities are greater than 0.5 through conditional judgment. Then we get the final linear equation by linear regression of the coordinate set. WELSCH loss instead of mean square loss(L2) is used to weaken the influence of several outliers. The commonly used distance metrics in linear regression are L2, L1, L12, FAIR, HUBER,

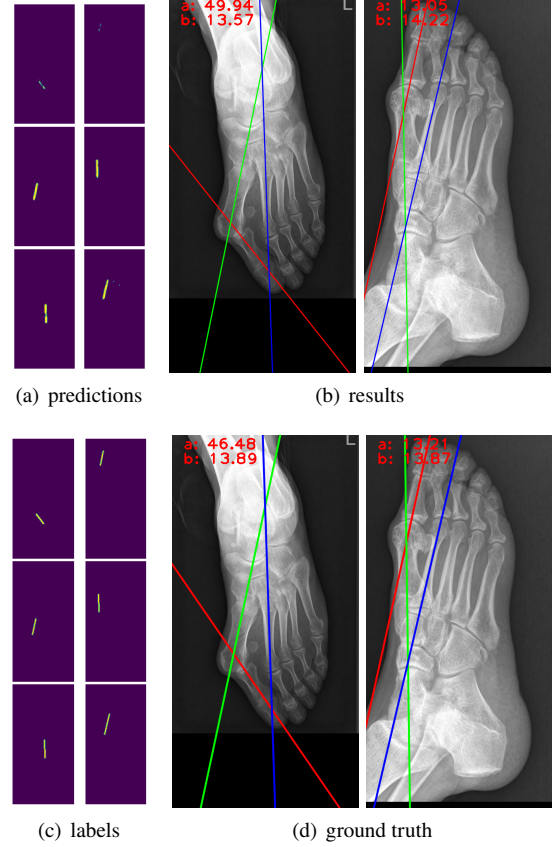


**Figure 7:** The results of our method. Fig (a) is the predicted heatmaps of neural network; (b) is the final results after linear regression; (c) is the labels for neural network; (d) is the ground truth.

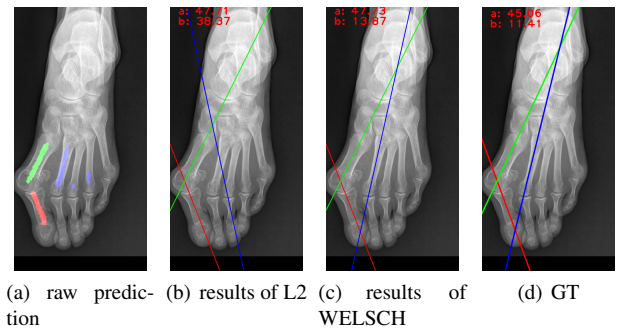


**Figure 8:** Comparison of Regression results of Different Distance Metrics

WELSCH. L2 is too sensitive to outliers, L1, L12, FAIR and HUBER are linear or nearly linear when the distance is far enough. Only WELSCH approaches a constant as the distance gets too far. Fig 8 is an example, (a) is the result of the network's predictions scaled and superimposed on the original image. The red ones and green ones are close to ground truth, but there are some outliers in the blue ones. When we take L2 as distance metric, the final result is as (b) shows, whose blue line is totally incorrect, when we take WELSCH instead, the results is much better as (c) shows.

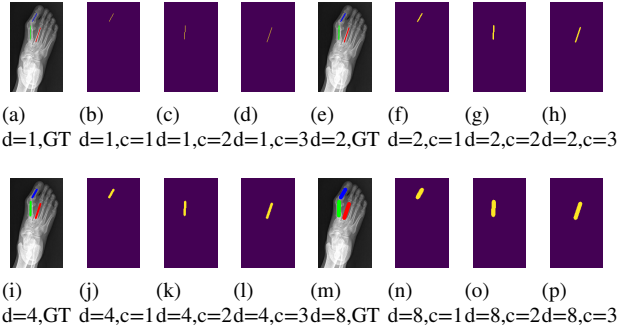


Figure 9: Ground Truth and Labels of Different Line Width

## 4. Experiments

### 4.1. Dataset

We collect a HVA dataset which include 230 preoperative images from 143 patients. We labeled two endpoints for every phalanx that needs attention. We draw the center lines and calculated the angles  $\alpha$  and  $\beta$  for every image like 7 (d) shows. Here  $a$  is  $\alpha$ ,  $b$  is  $\beta$ . Anyone who wants to make a better model can intuitively see the difference between their predictions and ground truth. In our experiments, we take 150 samples as training dataset, the rest 65 images as test dataset.

### 4.2. Evaluation Metrics

Because there are no ready-made evaluation metrics for our task, we developed a metric by ourselves. For this task, the most important goal is to get accurate and reliable angles. Mean angle errors(MAE) are first come to our mind, but there is an problem, it's very susceptible to outliers. For example, there are 10 samples and two method. For the first method, one of the results deviates by 90 degrees, the others deviates by 1 degree, then MAE becomes 9.9 degrees. For the second method, all of the results deviated by 9.9 degrees, so MAE is also 9.9 degrees. These two methods are indistinguishable under MAE. However, for surgeon, the first method have 9 acceptable results while the second has none. Therefore, we made a metric  $acc^t$  which can present the accuracy of predicted angle errors less than some threshold. The metric is as follows:

$$acc^t = \frac{1}{total} \sum_{i=1}^{total} (P(X[i]) - G(X[i]) < t) \quad (1)$$

Where  $t$  is an angle threshold,  $total$  is the number of samples of dataset,  $X$  is the images of dataset,  $P(X[i])$  is the predicted angles,  $G(X[i])$  is the manually annotated angles.

### 4.3. Comparison of Different Line Width

We also take line width into consideration. A larger line width can make the trained network more robust, but at the same time it will also introduce more inherent deviations, especially for line segments with a smaller line length. The ground truth and labels of different line width are shown in 9. Just looking at it with the naked eye, choosing a line width

Table 2

Comparison of Different Line Width on Test Dataset (Red is the best)

Line Width	$acc_{\alpha}^{3^{\circ}}(\%)$	$acc_{\alpha}^{5^{\circ}}(\%)$	$acc_{\beta}^{3^{\circ}}(\%)$	$acc_{\beta}^{5^{\circ}}(\%)$
1	46.15	61.54	72.31	86.15
2	50.77	61.54	70.77	80.00
3	49.23	66.15	73.85	86.15
4	<b>76.92</b>	89.23	<b>83.08</b>	<b>100.00</b>
5	60.00	70.77	73.85	84.62
6	58.46	<b>90.77</b>	73.85	89.23

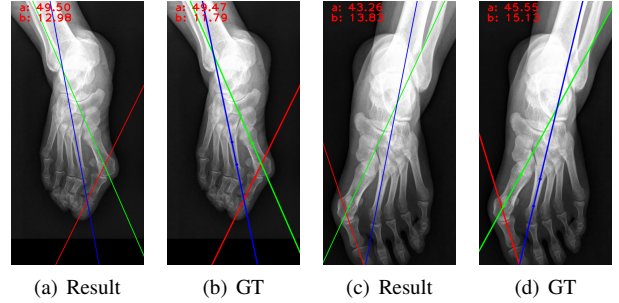


Figure 10: Results with  $Error_{\alpha} < 3^{\circ}$

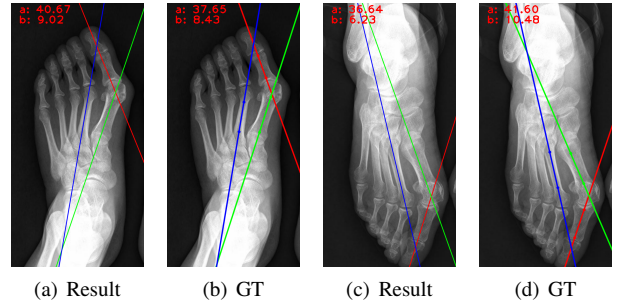


Figure 11: Results with  $3^{\circ} < Error_{\alpha} < 5^{\circ}$

of 4 may be a good choice. To determine which line width is best, we did a comparative experiment. The results are shown in Tab 2,  $acc_{\alpha}^{3^{\circ}}$  means the accuracy of the prediction error of  $\alpha < 3^{\circ}$ , the rest is similar. In general, it is indeed the best result when the line width is 4. From the Tab 2, we can also find that the accuracy of  $\beta$  is always higher than  $\alpha$ . It may because the phalanx corresponding to  $\beta$  are more slender which makes them easier to predict.

### 4.4. Results

Good results are shown in Fig 10, slightly worse results are shown in Fig 11. Failure cases are shown in 12, it failed because the red ones didn't predicted well. If there are more training samples available, this kind of failure cases will be improved.

### 4.5. Impletation Details of our method

For our neural network, the input size is  $1024*512*3$  and the output size is  $256*128*3$ . It's worth noting that the orig-

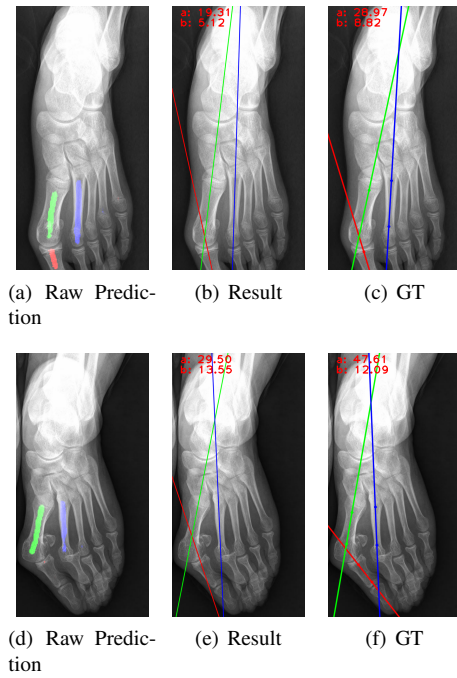


Figure 12: Results with  $Error_{\alpha} > 5^{\circ}$

inal size and aspect ratio of the input images is various. In order to zoom the image to the same size without distortion, we first scale the image proportionally to a width of 512, then or images with a height greater than 1024, we crop the excess, and for images with a height less than 1024, we fill in black pixels to a height of 1024. The output channels of neural network correspond to three line segments as Fig 7 shows. The optimizer for neural network is RMS, the initial learning rate is  $5E-5$ , the loss function is binary cross entropy, and the activation function of the output layer is sigmoid.

## 5. Summary

To make the HVA measurement more automatic and intelligent, we collect a dataset which include 235 preoperative images from 143 patients. And we designs a two-stage method combined with deep learning and linear regression, which can carry out high-precision prediction of HVA and IMA.

Future work:

1. Making a large-scale foot bone dataset based on virtual simulation.
2. Based on the transfer learning method, making the large-scale training model in the virtual scene can be well transferred to the real scene.
3. Extending the scene to postoperative HVA measurements and other bone angle measurements based on X-ray images.

## 6. Acknowledgement

This work was supported by the Ningbo Science and Technology Innovation Project [grant number No.2020Z019]; the

Huamei Fund [grant number 2019HMKY10]; and the Zhejiang Medical Fund [grant number 2020KY843].

## References

- [1] R. Alvarez, R. J. Haddad, N. Gould, S. Trevino, The simple bunion: anatomy at the metatarsophalangeal joint of the great toe, *Foot & ankle* 4 (1984) 229–240.
- [2] S. Nix, M. Smith, B. Vicenzino, Prevalence of hallux valgus in the general population: a systematic review and meta-analysis, *Journal of foot and ankle research* 3 (2010) 1–9.
- [3] G. Spahn, R. Schiele, A. Hell, H. Klinger, The prevalence of pain and deformities in the feet of adolescents. results of a cross-sectional study, *Zeitschrift fur Orthopadie und ihre Grenzgebiete* 142 (2004) 389–396.
- [4] F. Benvenuti, L. Ferrucci, J. M. Guralnik, S. Gangemi, A. Baroni, Foot pain and disability in older persons: an epidemiologic survey, *Journal of the American Geriatrics Society* 43 (1995) 479–484.
- [5] H. B. Menz, S. R. Lord, Gait instability in older people with hallux valgus, *Foot & ankle international* 26 (2005) 483–489.
- [6] H. B. Menz, S. R. Lord, The contribution of foot problems to mobility impairment and falls in community-dwelling older people, *Journal of the American Geriatrics Society* 49 (2001) 1651–1656.
- [7] K. Koski, H. Luukinen, P. Laippala, S.-L. Kivela, Physiological factors and medications as predictors of injurious falls by elderly people: a prospective population-based study, *Age and ageing* 25 (1996) 29–38.
- [8] E. Wagner, C. Ortiz, K. Torres, I. Contesse, O. Vela, D. Zanolli, Cost effectiveness of different techniques in hallux valgus surgery, *Foot and Ankle Surgery* 22 (2016) 259–264.
- [9] N. Heineman, G. Liu, T. Pacicco, R. Dessouky, D. K. Wukich, A. Chhabra, Clinical and imaging assessment and treatment of hallux valgus, *Acta Radiologica* 61 (2020) 56–66.
- [10] C. Piqué-Vidal, J. Vila, A geometric analysis of hallux valgus: correlation with clinical assessment of severity, *Journal of foot and ankle research* 2 (2009) 1–8.
- [11] K. M. Lee, S. Ahn, C. Y. Chung, K. H. Sung, M. S. Park, Reliability and relationship of radiographic measurements in hallux valgus, *Clinical Orthopaedics and Related Research* 470 (2012) 2613–2621.
- [12] M. J. Coughlin, E. Freund, The reliability of angular measurements in hallux valgus deformities, *Foot & ankle international* 22 (2001) 369–379.
- [13] T. D. Chi, J. Davitt, A. Younger, S. Holt, B. J. Sangeorzan, Intra- and inter-observer reliability of the distal metatarsal articular angle in adult hallux valgus, *Foot & ankle international* 23 (2002) 722–726.
- [14] E. P. Cruz, F. V. Wagner, C. Henning, J. A. V. Sanhudo, F. Pagnusato, C. R. Galia, Comparison between simple radiographic and computed tomographic three-dimensional reconstruction for evaluation of the distal metatarsal articular angle, *The Journal of Foot and Ankle Surgery* 56 (2017) 505–509.
- [15] P. van der Woude, S. B. Keizer, M. Wever-Korevaar, B. J. Thomassen, Intra- and interobserver agreement in hallux valgus angle measurements on weightbearing and non-weightbearing radiographs, *The Journal of Foot and Ankle Surgery* 58 (2019) 706–712.
- [16] M. Dantone, J. Gall, C. Leistner, L. Van Gool, Human pose estimation using body parts dependent joint regressors, in: *Proceedings of the IEEE Conference on Computer Vision and Pattern Recognition*, 2013, pp. 3041–3048.
- [17] G. Gkioxari, P. Arbeláez, L. Bourdev, J. Malik, Articulated pose estimation using discriminative armllet classifiers, in: *Proceedings of the IEEE Conference on Computer Vision and Pattern Recognition*, 2013, pp. 3342–3349.
- [18] A. Toshev, C. Szegedy, Deeppose: Human pose estimation via deep neural networks, in: *Proceedings of the IEEE conference on computer vision and pattern recognition*, 2014, pp. 1653–1660.
- [19] J. Carreira, P. Agrawal, K. Fragkiadaki, J. Malik, Human pose estimation with iterative error feedback, in: *Proceedings of the IEEE con-*

- ference on computer vision and pattern recognition, 2016, pp. 4733–4742.
- [20] X. Sun, J. Shang, S. Liang, Y. Wei, Compositional human pose regression, in: Proceedings of the IEEE International Conference on Computer Vision, 2017, pp. 2602–2611.
  - [21] A. Newell, K. Yang, J. Deng, Stacked hourglass networks for human pose estimation, in: European conference on computer vision, Springer, 2016, pp. 483–499.
  - [22] S.-E. Wei, V. Ramakrishna, T. Kanade, Y. Sheikh, Convolutional pose machines, in: Proceedings of the IEEE conference on Computer Vision and Pattern Recognition, 2016, pp. 4724–4732.
  - [23] J. Tompson, A. Jain, Y. LeCun, C. Bregler, Joint training of a convolutional network and a graphical model for human pose estimation, arXiv preprint arXiv:1406.2984 (2014).
  - [24] G. Papandreou, T. Zhu, N. Kanazawa, A. Toshev, J. Tompson, C. Bregler, K. Murphy, Towards accurate multi-person pose estimation in the wild, in: Proceedings of the IEEE Conference on Computer Vision and Pattern Recognition, 2017, pp. 4903–4911.
  - [25] U. Rafi, B. Leibe, J. Gall, I. Kostrikov, An efficient convolutional network for human pose estimation., in: BMVC, volume 1, 2016, p. 2.
  - [26] B. Xiao, H. Wu, Y. Wei, Simple baselines for human pose estimation and tracking, in: Proceedings of the European conference on computer vision (ECCV), 2018, pp. 466–481.
  - [27] J. Tompson, R. Goroshin, A. Jain, Y. LeCun, C. Bregler, Efficient object localization using convolutional networks, in: Proceedings of the IEEE conference on computer vision and pattern recognition, 2015, pp. 648–656.
  - [28] A. Bulat, G. Tzimiropoulos, Human pose estimation via convolutional part heatmap regression, in: European Conference on Computer Vision, Springer, 2016, pp. 717–732.
  - [29] W. Yang, S. Li, W. Ouyang, H. Li, X. Wang, Learning feature pyramids for human pose estimation, in: proceedings of the IEEE international conference on computer vision, 2017, pp. 1281–1290.
  - [30] V. Belagiannis, A. Zisserman, Recurrent human pose estimation, in: 2017 12th IEEE International Conference on Automatic Face & Gesture Recognition (FG 2017), IEEE, 2017, pp. 468–475.
  - [31] K. Sun, B. Xiao, D. Liu, J. Wang, Deep high-resolution representation learning for human pose estimation, in: Proceedings of the IEEE/CVF Conference on Computer Vision and Pattern Recognition, 2019, pp. 5693–5703.